Study and Hardware Implementation of Floating Multiphase Boost Converter for Fuel Cell Electrical Vehicle

Slah Farhani*, El Manaa Barhoumi**‡, Faouzi Bacha***, Abdeslem Djerdir****

*LISI Laboratory, INSAT, University of Carthage, B.P. 676, 1080 Tunis Cedex, Tunisia

** Department of Electrical and Computer Engineering, College of Engineering, Dhofar University, Salalah, Oman

*** Department of Electrical Engineering, ENSIT, University of Tunis, Tunisia.

**** Department of Energy, Laboratory research FCLAB, University of Technology at Belfort and Montbéliard, France.

(slah.farhani@isetkr.rnu.tn, ebarhoumi@du.edu.om, faouzi.bacha@esstt.rnu.tn, abdesslem.djerdir@utbm.fr)

‡ Corresponding Author; El Manaa Barhoumi, Dhofar University, Oman, Tel: +96898190380, Fax: + 21677 323 320, ebarhoumi@du.edu.om

Received: 15.06.2022 Accepted:16.08.2022

Abstract- The aim of this paper is the modelling and the implementation of a floating interleaved boost converter for proton exchange membrane fuel cell vehicle application. The fuel cell vehicle represents a credible solution for electrical transportation. To rise the voltage generated by the fuel cell to a suitable voltage required by the electrical motor, the boost converter represents a competitive technical solution. Furthermore, the interleaved boost converter allows the reduction of the voltage ripples and the increase in the fuel cell life time. The floating structure has the highest voltage gain and efficiency compared to other boost converters. Floating interleaved boost converter is a reassuring structure of the boost converters to interface the fuel cell with continues bus in a combined power train. The current paper mainly focuses on the development of fuel cell power converters applications through the enhancement of the voltage gain and efficiency. This converter proves its efficiency at the level of reducing ripple input current as well as maintaining high voltage gain and low voltage ripple. Eventually, the performances of the proposed converter evaluate using an experimental prototype. Despite the analysis and control of power converters were widely developed, the implementation of the control of the power converter using Dspace and FPGA is presented for the first time in this paper. The experimental results show the ability of the converter to reduce the input current ripple for different power range and reduce the current stress and power loss of different components.

Keywords Floating interleaved converter, fuel cell, electric vehicle, experimentation.

1. Introduction

The excessive use of fuel, natural gazes and coal has caused an important diminution of fossil fuels as well as environmental pollution [1]–[4]. To reduce the effect of using non renewable energy sources, new policies have been developed to encourage the exploitation of renewable energy sources to produce electrical power [5]. However, the storage of electrical energy produced from renewable sources remains the main issue of using these sources in an effective manner [6], [7]. Moreover, the increase in population, the industrial development and the urbanization growth has triggered researchers to find optimistic solution for the above-mentioned issues [8], [9]. The use of the Fuel Cell (FC) as an electrical generator is considered an optimal solution [10]–[12]. The FC allows the generation of electrical energy from hydrogen stored in special tanks. Moreover, renewable energy sources like solar and wind power are used to produce hydrogen [13]–[15]. For such reason, FCs have been used in different industrial applications like automotive and portable applications [16]–[19]. Currently, the electrical vehicle has attracted the attention of industry consistencies

and researchers in renewable energy systems [20], [21]. The FC is proposed as an electrical generator for the fuel cell vehicle. Usually, the fuel cell vehicle is based on the use of FC, battery, super capacitors and power converters [16], [18], [19], [22], [23]. The role of the DC/DC converters and inverters is to control the flow of the power in an effective way[20]. The general structure of the electrical vehicle system is shown in Fig.1 [18].

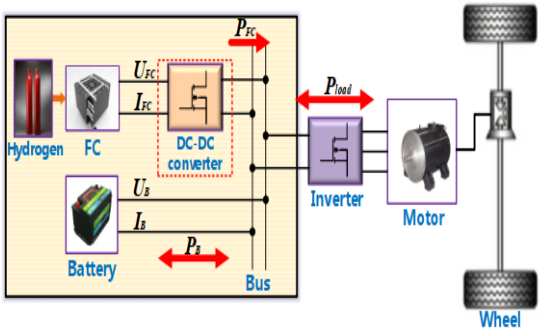

Fig. 1. General structure of electric vehicle system.

The FC is a specific generator having non-linear characteristic of voltage-current [12]. The voltage decreases when the current increases and the produced power is maximized at a specific defined current. Furthermore, the current and voltage ripples affect the FC life time [24]. For this reason, the design of specific power converters became a necessity to improve the reliability, efficiency and lifetime of FC systems. The classic boost converter allows the stepping up of the FC voltage to be adequate to the required load voltage [25]. However, the minimization of voltage and current ripples requires a big-sized capacitor and inductors [20]. This solution represents a major drawback for the portable applications like electrical vehicle systems. The aim of the interleaved boost converter is rise the voltage and keep minimum sizes of the capacitor and the inductor [24]. These converters are made of classic boost converters structures connected in parallel [26]. In this way, they require a specific control approach to reduce the current ripples. This approach permits to minimize the FC current ripples and improve the FC lifetime.

Usually, the load requires high voltage compared to the one produced by the FC. Then, the floating structure of interleaved boost converters creates a credible solution to increase the output voltage and reduce the current ripples at the same time [27]. The floating interleaved boost converter (FIBC) is mainly based on the use of the two structures of two phases interleaved boost converters. The two interleaved converters are connected in anti-parallel to the same load. This allows the considerable increase of the output voltage even when working at low duty cycle. Furthermore, the FIBC has many advantages compared to other classic interleaved boost converters. Indeed, the FIBC is considered has high efficiency and lower passive devices than multiphase interleaved boost converter. The FIBC permits the production of the required voltage with a minimum size of passive components. The size of the inductors and capacitor in FIBC is equal to the half the size of components used in interleaved boost converter and equals quarter the size of passive components used in the classical structure. Even though the FIBC used more passive components compared to other boost converters topologies, the FIBC is recommended in the DC/DC conversion thanks to its high efficiency and high voltage gain. Moreover, the FIBC is characterized by less voltage stress on power switches (e.g., switches, diodes). In addition, some other advantages are higher switch utilization factors, lower switching stress, smaller inductor volumes thanks to lower current flow through each inductor, lower capacitor voltage ratings, as each capacitor carries only about 60% of the output voltage, and lower power losses and less voltage drop across the inductors [28]. Thanks to all these advantages, the FIBC represents a competitive solution for electrical vehicle applications [29].

The analysis of the technology of power converters for the control of the power flow of the FC show that a wide range of converters is developed in the literature. However, the FIBC was not analyzed and its control is not well investigated. The control of boost converters using DSpace shows good performances in terms of response time and accuracy [30]. The DSpace permits to generate different signals required for the control of the power switches. The energy management system of FC renewable energy system can be developed using Matlab and implemented using Microntroller [31]. The FPGA represents an interesting technology developed for the control of power converters [32]. Using Dspace and FPGA technologies will be developed in this paper to control an FIBC. Eventually, this paper proposes the analysis and the experimental validation of the use of the FIBC in electrical vehicle application. This paper is organized into five main sections. The introduction is presented in the first section. The second section displays the model and the electrical equivalent circuit of the used PEMFC. In the third section, the FIBC structure is presented and analyzed. The mathematical model is presented and discussed in the same section. The simulation and experimental results as well as the test bed are presented and discussed in section four. Furthermore, the conclusion is presented in the fifth section.

2. Fuel cell Modeling

The PEMFC is an electrochemical system that converts chemical energy (Hydrogen) into electrical energy through a chemical reaction of hydrogen and oxygen [33]. Without using thermal or electromechanical conversion system, both oxygen and hydrogen are converted into water and electricity through the procedure of turning chemical energy into electrical energy. Under the influence of the electric field, the fuel cell is able to settle both the anode and the cathode separated by the electrolyte. Such settlement enables the ions to move freely between electrodes.

In overall, the basic principle of operation of the PEMFC has been considered as dual chemical reaction composed of oxidation and reduction reactions taking place at the anode and the cathode, respectively. At the anode, there is a whole process of oxidizing hydrogen into two protons and two electrons. At the cathode, the two protons and the two

electrons reduce oxygen to water. The overall chemical reaction is described by expression (1) [11].

$$H_2 + \frac{1}{2}O_2 \rightarrow 2H_2O + electrical\ energy + heat\ energy \quad (1)$$

The generated voltage of the PEMFC is described as [10]:

$$V_{FC} = E_{Nernst} - V_{act} - V_{ohmic} - V_{con} \quad (2)$$

Where V_{Act} is used for modeling the activation losses and is given as [15]:

$$V_{Act} = A.ln\left(\frac{i_{FC} + i_n}{i_0}\right) \quad (3)$$

The voltage drop due to Ohmic losses is expressed as:

$$V_{Ohm} = R_m(i_{FC} + i_n) \quad (4)$$

The concentrations losses are expressed as:

$$V_{Con} = -B.ln\left(1 - \frac{i_{FC} + i_n}{i_l}\right) \quad (5)$$

The electrical equivalent circuit used for modeling the PEMFC is depicted in Fig. 2.

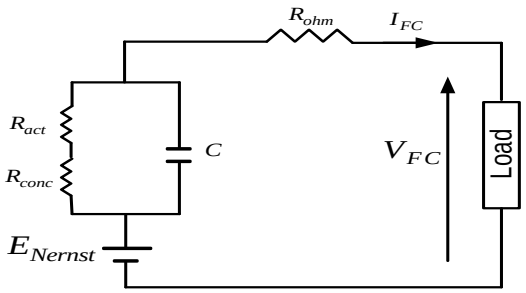

Fig. 2. Electrical equivalent circuit

Fig. 3 explicitly translates relation (1) wherein the double-larger charge is the principal cause behind the gap between the activation voltage and the concentration voltage represented by the resistance Ract and the resistance Rconc, respectively. It is also worth noting that the accumulation of charges between two different materials is fundamental condition to this phenomenon. The behavior of the charge layer in the Electrode/electrolyte interface is similar to that of a capacitor.

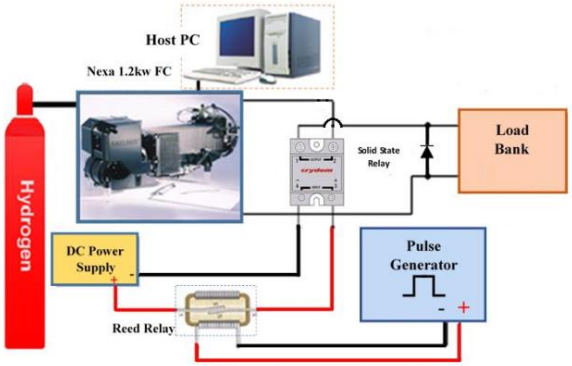

Fig. 3. Schematic representation

In this study, experiments are conducted with Ballard Nexa 1200 fuel cell module under the diverse operating situation, whether static or dynamic ones. A symbolic representation of the PEMFC test bed is shown in Fig. 4. The test bench is mainly made up of PEMFC Ballard Nexa, hydrogen tank equipment with all components i.e., inlet valve, pressure regulating pressure-regulating valve, and exhaust gas electromagnetic valve. An electronically controlled load is used to emulate electric vehicle behavior. A photograph of the test bed is depicted in Fig. 4.

Fig. 4. Photograph of the test bed

The practical bench which allows the plotting of the polarization curveting is presented in Fig.5. The current and the voltage variation of the PEMFC have been the main objective of this first experiment. Moreover, this experiment basically focuses on the observation of the fuel cell electric model behavior and the assessment of its performance. The 26 V direct current was obtained at a current of 45A and an ambient temperature of 25°C. The rated power is about 1200W considered as the maximum stack power obtained at normal working conditions of the PEMFC. Fig. 6 illustrates the polarization characteristics, of the PEMFC. The obtained polarization curves are identical to the characteristics provided in the datasheet. The produced output power by the PEMFC is calculated using the values of the voltage and the current. The obtained results of the power are presented in Figure 6. The maximum power of the PEMFC, 1.2 kW, corresponds to a maximum current of 45 A.

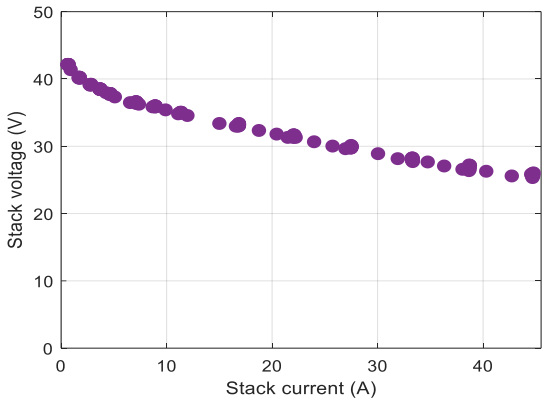

Fig. 5. Practical characteristic

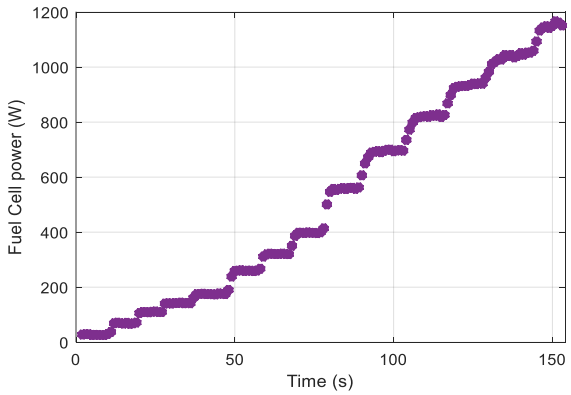

Fig. 6. Power, run up operation

3. Floating Interleaved boost converter

3.1. Converter Topology

The interleaving conception, on which the implied topology is established and ensured by the common inputs' connection of a non-floating and a floating converter and the shift of the command signals for the power semiconductors (S1, S2, S3, and S4). Incorporating more than two converter phases permits the minimization of the source current ripples. Moreover, this topology reduces the electrical constraints on the power semiconductors. The phase number interleaved phases of the power converter must be always equal in aim to hold the equilibrium among the top part (i.e. non-floating part) and the bottom part (i.e. floating element). In addition, from a point of view of dependability, this structure is a vigorous addition compared to the two phase's interleaved converter. The FIBC presented in Fig.7 is based on the use of two structures of two phases interleaved boost converter. The two phases interleaved boost converters are connected in anti-parallel to a common DC bus voltage. The control signals generated to turn on-off the switches are shifted by T/n where n is the number of legs of the converter.

To compare the classical boost converter, the advantages of the floating interleaved topology are set down beneath:

- The size and volume of inductors and capacitors components are minimized.
- The output voltage and current ripples are decreased considerably compared to classic structures.
- The voltage and current ripples disappear completely for particular duty cycle value
- d = a / n where a varies from 1 to n-1, according to the number of legs of the FIBC.
- The frequency of the input current ripple is raised.
- Although the converter is modular, it makes perfectly the system reliable due to the existence of additional freedom degrees and increases the converter power through the parallel phase's connection.
- Thermal management operation is straightforward.
- Making the phases parallel allows a leading thermal distribution.

The semiconductors' currents of the power are minimized owing to the converter interleaving.

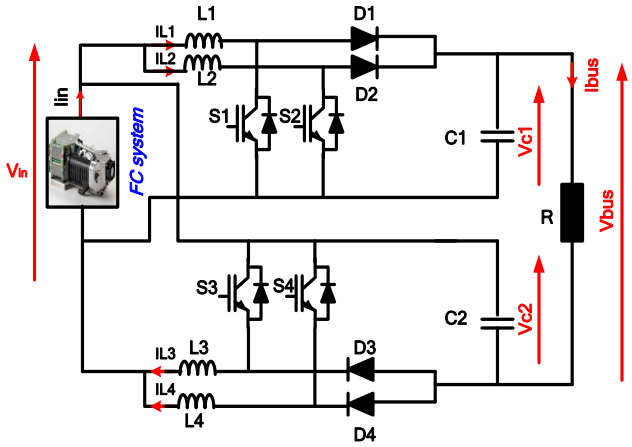

Fig. 7. FIBC topology

3.2. Converter Modelling

To ensure the converter control and the performance targets, suitable dynamic models of the used topology are necessary. For the sequences of operation defined by (0 <t <DTs) and (DTs <t <Ts), the dynamic current equations are expressed as:

$$\frac{dI_{L1}}{dt}=\frac{(d-1)}{L}V_{C1}+\frac{1}{L}V_{FC}$$
$$\frac{dI_{L2}}{dt}=\frac{(d-1)}{L}V_{C1}+\frac{1}{L}V_{FC}$$
$$\frac{dI_{L3}}{dt}=\frac{(d-1)}{L}V_{C2}+\frac{1}{L}V_{FC}$$
$$\frac{dI_{L4}}{dt}=\frac{(d-1)}{L}V_{C2}+\frac{1}{L}V_{FC} \quad (6)$$
$$\frac{dV_{C1}}{dt}=\frac{(d-1)}{L}I_{L1}+\frac{(d-1)}{L}I_{L2}-\frac{1}{RC}V_{C1}-\frac{1}{RC}V_{C2}+\frac{1}{RC}V_{FC}$$
$$\frac{dV_{C2}}{dt}=\frac{(d-1)}{L}I_{L3}+\frac{(d-1)}{L}I_{L4}-\frac{1}{RC}V_{C1}-\frac{1}{RC}V_{C2}+\frac{1}{RC}V_{FC}$$

The fuel cell current depends on the different currents in the inductors and the bus current. Thus, the FC current and the DC bus voltage are expressed as:

$$\frac{dI_{in}}{dt}=\sum_{i=1}^{4}\frac{dI_{Li}}{dt}-\frac{dI_{bus}}{dt}$$
$$\frac{dV_{bus}}{dt}=\sum_{i=1}^{2}\frac{dV_{ci}}{dt}-\frac{dV_{in}}{dt} \quad (7)$$

3.3. Converter Design

The FIBC allows the reduction of the current ripples since the current is divided into four phases. This permits the use of inductors with less size and volume. The reduction of the inductor current ripple is obviously achieved though the combination of the interleaving concept and the phase shift of 360/N between the control signals.

As a consequence, there is a vital necessity to lower both the inductor value and its volume. In order to reduce the size and weight, it is imperative to decrease the passive components as well as heat sink. Fig.4 below illustrates the switches gates signals. It also depicts the current of the input, the inductor as well as the capacitors. The output voltage for a duty cycle (50% < D < 75%) is also highlighted in Fig.8.

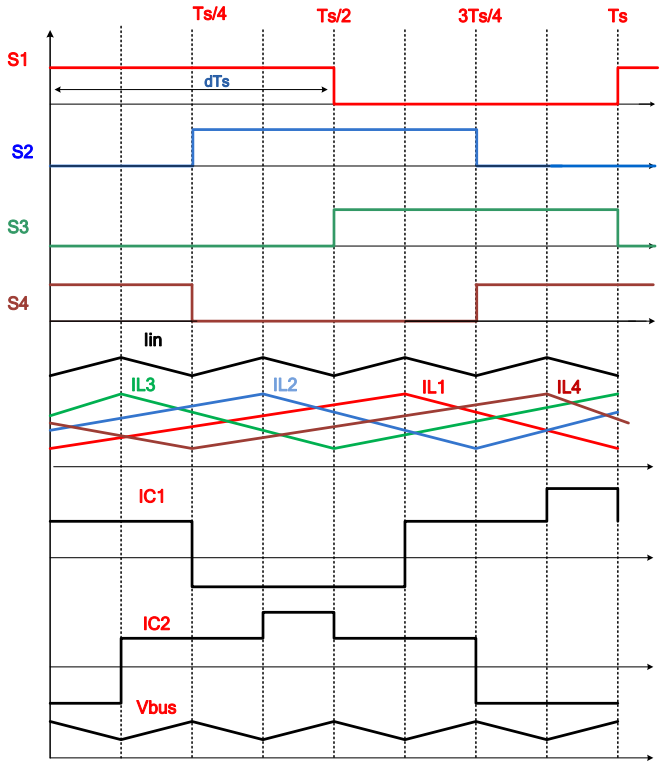

Fig. 8. Waveforms of a four-phase FIBC

From Fig. 4 and during the interval (Ts/2 < t < 5Ts/8), the following equations can be written.

$$\frac{di_{L1}}{dt}=\frac{V_{fc}}{L_1}$$
$$\frac{di_{L2}}{dt}=\frac{V_{fc}}{L_2}$$
$$\frac{di_{L3}}{dt}=\frac{V_{fc}}{L_3} \quad (8)$$
$$\frac{di_{L4}}{dt}=\frac{V_{fc}-V_{c2}}{L_4}$$

$$\frac{dV_{c1}}{dt}=-\frac{I_0}{C_1}$$
$$\frac{dV_{c2}}{dt}=\frac{I_{fc}-3I_0}{4C_2} \quad (9)$$

The input current and dynamics of the DC-bus voltage are described below.

$$\frac{di_{fc}}{dt}=\frac{di_{L1}}{dt}+\frac{di_{L2}}{dt}+\frac{di_{L3}}{dt}+\frac{di_{L4}}{dt}-\frac{di_0}{dt}$$
$$\frac{dV_{Bus}}{dt}=\frac{dV_{c1}}{dt}+\frac{dV_{c2}}{dt}-\frac{dV_{fc}}{dt} \quad (10)$$

Using equations (8), (9) and (10), the inductor and the capacitor value can be obtained as follows

$$L=\frac{(3-4d)(d-0.5)V_{Bus}}{(1+d)\Delta V_{fc}\ f_s}$$
$$C=\frac{(3-4d)(d-0.5)V_{Bus}}{2(1-d)\,\Delta V_{Bus}\ Rf_s} \quad (11)$$

The inductor current ripple can be obtained by

$$\Delta i_L=\frac{d(1-d)V_{Bus}}{(1+d)Lf_s} \quad (12)$$

Table 1 presents the parameters used in this study.

Table 1. FIBC parameters

Parameter	Value
Fuel cell voltage	28V
DC bus	80V
Switching frequency	20KHz
Inductor	120µH
Capacitor	470µF

4. Results and discussion

4.1. Simulation results

This section presents the implemented scenario in order to verify the effectiveness of the proposed converter and control approach. The simulation of the PEMFC and the associated converter has been carried out using MATLAB Simulink environment.

Fig.9 underlines the simulation results for the control signal for the PWM at a duty cycle, d = 0.5 where it can be seen that these four signals are shifted between them by

T / 4.

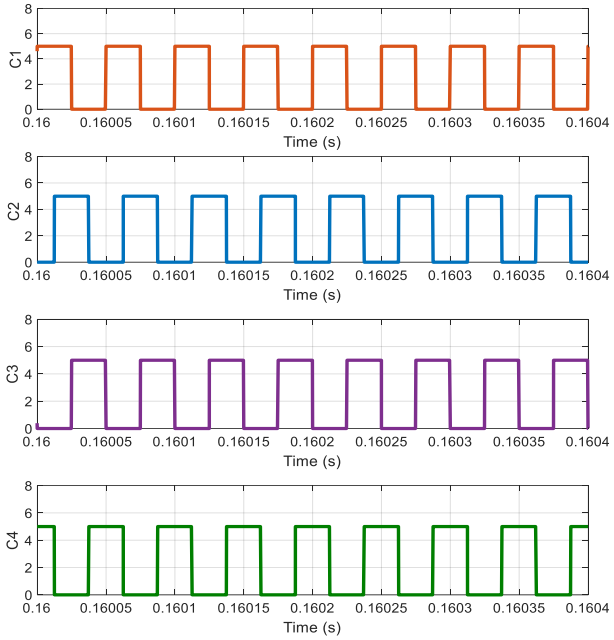

Fig. 9. Simulation PMW signals of a four-phase FIBC (d=0.5)

According to Fig.10, if the switch is on, the current inductance is increased linearly and decreased linearly as well as when the switch is off. These currents are shifted between them by T/4. The average values of the inductors currents are: iL1= iL4 = 5.2A, and iL2= iL3=9.7A. The input current is 22A and the output current is7.5A is shown in Fig.11.

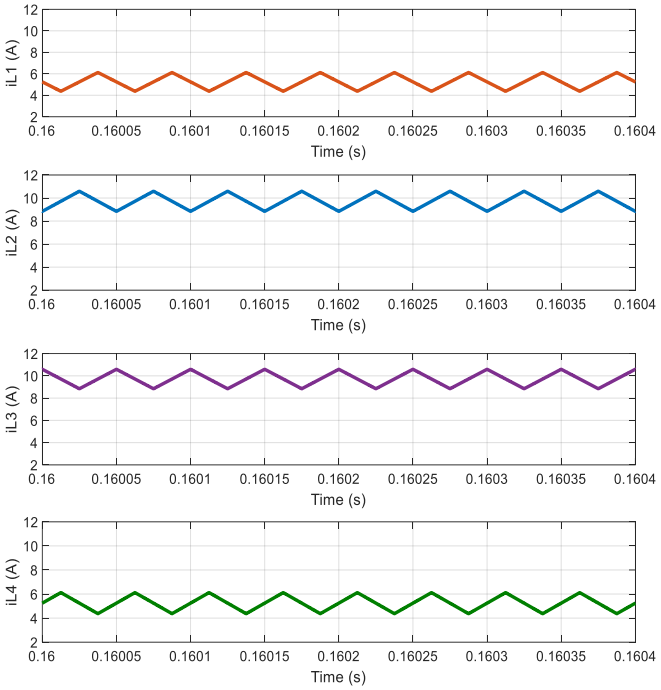

Fig. 10. Inductor currents waveforms of a four-phase FIBC (d=0.5)

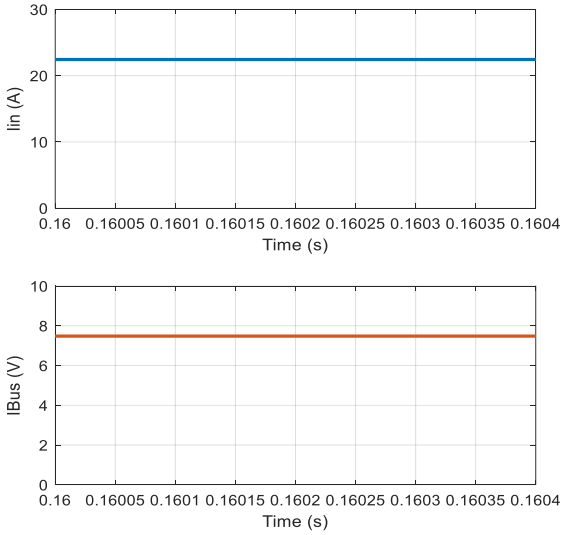

Fig. 11. Input and output currents waveforms of a four-phase FIBC (d=0.5)

The simulation result is obtained when the input voltage is 28V, the capacitor output voltage is 55V and the output voltage is 82V as shown in Fig.12.

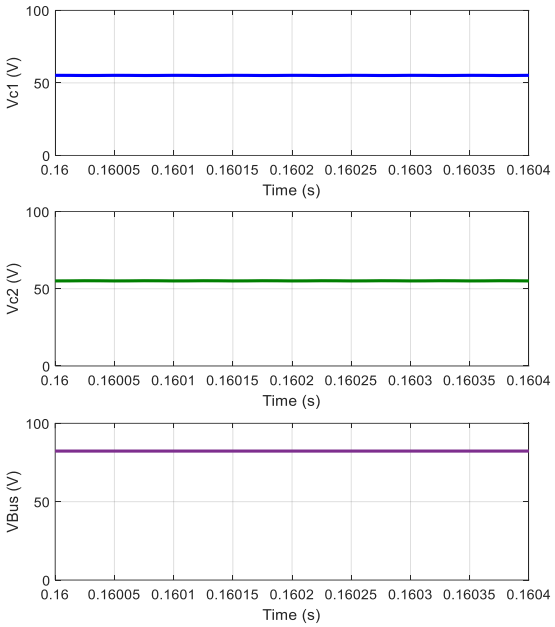

Fig. 12. Output voltages waveforms of a four-phase FIBC (d=0.5)

4.2. Experimental results

To validate the steady-state analysis performed in continuous conduction mode, a prototype of the converter circuit shown in Fig.7 is equally designed and tested in the laboratory. The experimental platforms of Floating Interleaved boost Converter (FIBC) are shown in Fig.13. The converter prototype is driven with a switching frequency of 20 kHz and the operating duty cycle is 0.5

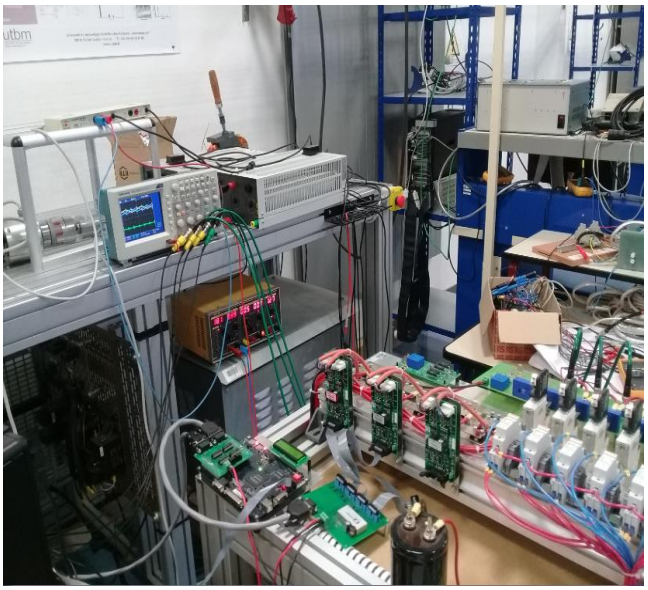

Fig. 13. Experimental platforms of Floating Interleaved boost Converter (FIBC)

The improved control system of the interleaved topologies with MATLAB/SIMULINK has been transmitted through the actual time board DSpace1104. The power switching signals are generated involving MATLAB with dSPACE (RTI 1104) controller. Nonetheless, these control signals are in phase as illustrated in Fig.14. In parallel with the structure of this research, the monitoring signals from the PWM port are modified by an FPGA board, as indicated in Fig.15. The FPGA is a VHDL calculation code which depends on the Altera Quartus II software. It is responsible for the activation of the port control- shift. Fig.16 clearly shows the operation of the system.

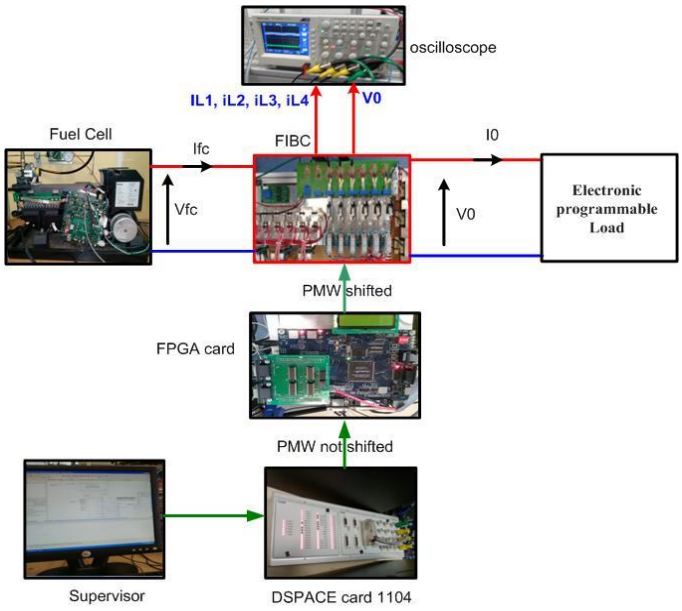

Fig. 14. Experimental platforms of Floating Interleaved boost Converter (FIBC)

The control signals shifting is set up on a parameter determined in the VHDL program and called shift value as shown by the following relation

$$shift_{value} = \frac{T_s}{\frac{360}{q}}.10^7$$

The above mentioned equation includes Ts as the switch operating time as well as θ as the shift angle of the control signal of the IBC converter. The latter is 90° taking into account the four-phase floating interleaved topology.

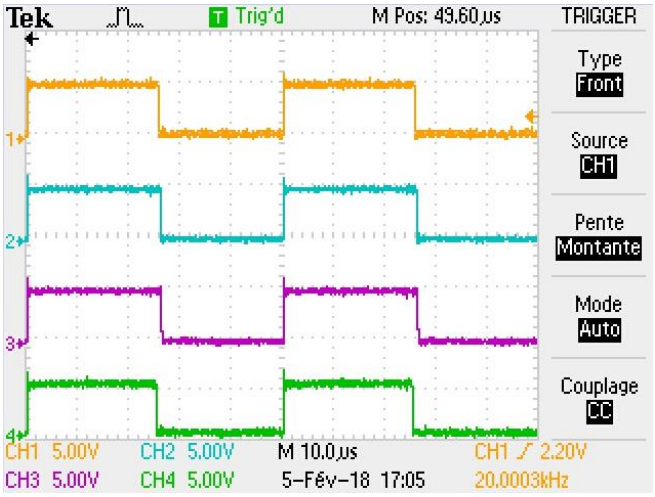

Fig. 15. Steady state switch control signals with 50% duty cycle produced by DSpace 1104

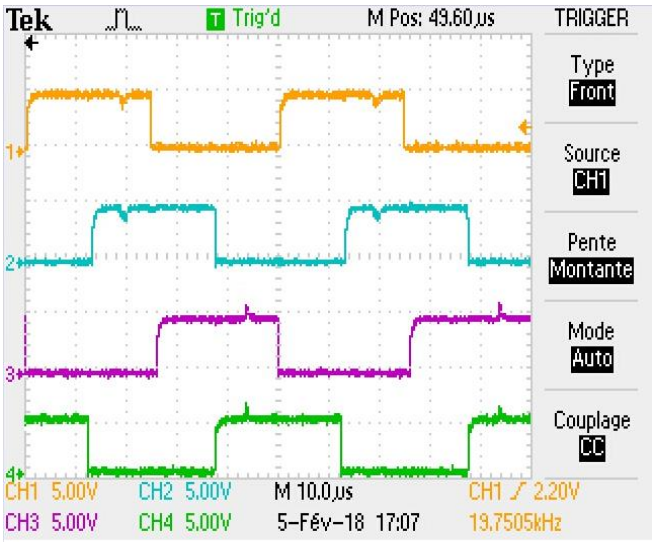

Fig. 16. Steady-state switch driving signals with 50% duty cycle and 90◦ out of phase from each other with FPGA board

The steady-state waveforms of the current variation show the ability of the four-phase FIBC to minimize the current ripples. It is possible to shift from a high current ripple in the inductors to a low value of order 4A at the input of the converter. Fig.17 exposes the inductance currents for the duty cycle; d = 0.5. They are shifted from each other by T / 4 and almost the same average values as in the simulation. Fig.18 shows the PWM signals (PMW1 and PMW2) and inductor currents (iL1 and iL2) of proposed convector (FIBC) for the duty cycle; d = 0.5.

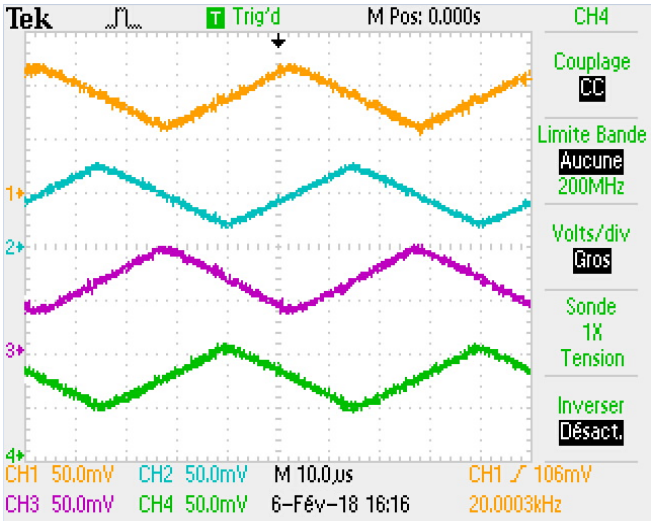

Fig. 17. Experimental inductor currents waveforms of a four-phase FIBC (d=0.5)

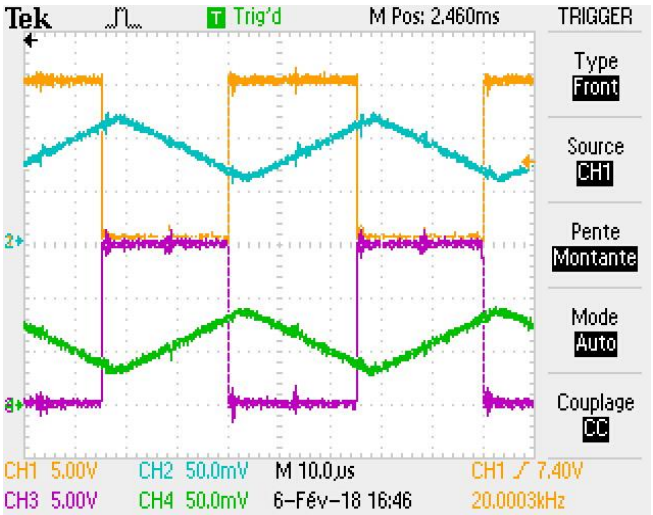

Fig. 18. Experimental PWM signals (PMW1 and PMW2) and inductor currents (iL1 and iL2)

From Fig.19, the total input current is 20 A, the inductance currents iL1 and iL4, and the output current through the load is 7A. The variation of the voltage of the output capacitor is shown in Fig.20; the value of this voltage is close to 54V.

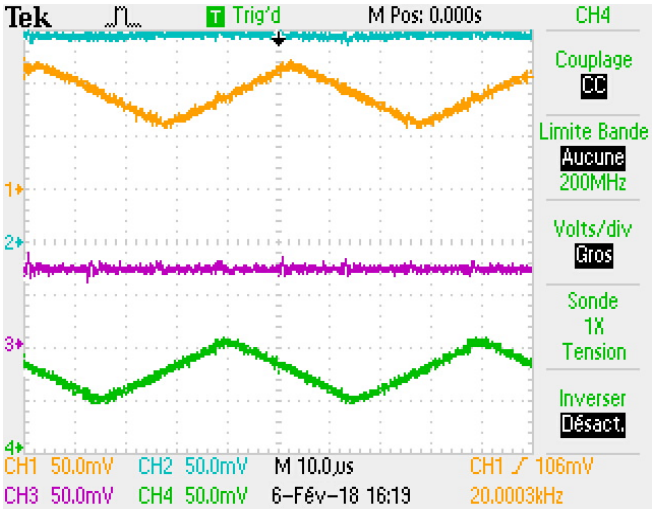

Fig. 19. Experimental PWM signals (PMW1 and PMW2) and inductor currents (iL1 and iL2)

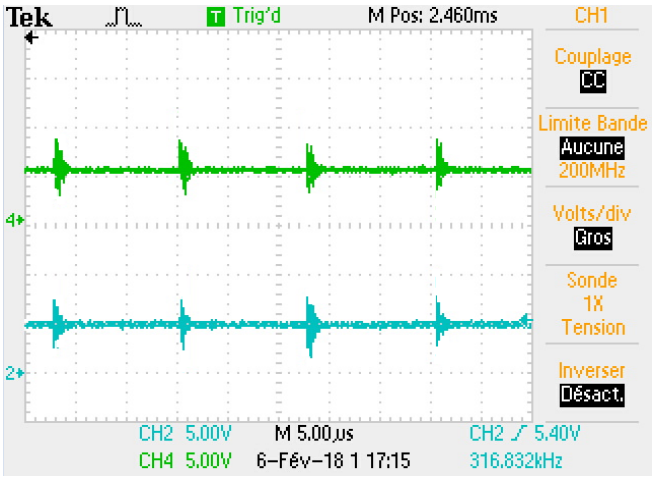

Fig. 20. Experimental PWM signals (PMW1 and PMW2) and inductor currents (iL1 and iL2)

It is obvious that the experimental and simulation results show a good agreement. In addition, there is proportionality between the progress of the output voltage and the duty cycle which is verified by the following theoretical equation:

$$d = \frac{V_{Bus} - V_{FC}}{V_{Bus} + V_{FC}}$$

Fig. 21 shows the efficiency curve of the proposed converter versus the output power; the input voltage is set to 28V and the duty cycle is 0.5. The four-phase FIBC topology allows improving the efficiency and reducing the current ripples. The converter has also shown a considerable reducing of the size of both the inductor and the capacitor components. This optimized structure leads eventually to a considerable minimization of switching and conducting losses.

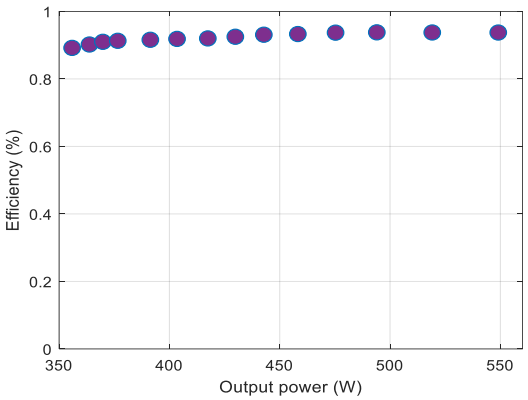

Fig. 21. Experimental efficiency of a four-phase FIBC

5. Conclusion

In this paper, a FIBC characterized by a minimum input current ripple has been presented and analyzed through simulations and experimental tests. The modeling of the converter is presented to analyze the variation of current and voltage in different components. The model shows that the converter allows the achievement of zero current ripples at higher output voltage. The principles of the operation and the ripple equations have been examined, and the components and semiconductors are equally selected. To validate the simulations results, a hardware prototype of the four-phase FIBC has been implemented, using a Dspace 1104 and an FPGA board. This prototype used IGBTs operating at a switching frequency of 20 kHz. The implemented converter has achieved an output power of 500W, such power has conducted 93% efficiency at duty cycle of 0.5 and 28V input voltage.

References

[1] S. Bahramara, M. P. Moghaddam, and M. R. Haghifam, "Optimal planning of hybrid renewable energy systems using HOMER: A review," *Renew. Sustain. Energy Rev.*, vol. 62, pp. 609–620, Sep. 2016, doi: 10.1016/j.rser.2016.05.039.

[2] A. Harrouz , A. Temmam, M. Abbes, "Renewable Energy in Algeria and Energy Management Systems," Int. J. Smart Grid, 2017, doi: 10.20508/ijsmartgrid.v2i1.10.g9.

[3] E. M. Barhoumi, P. Okonkwo, M. Zghaibeh, I. Ben Belgacem, T. Alkanhal, A. G. Abo-Khalil, I Tlili, "Renewable energy resources and workforce case study Saudi Arabia: review and recommendations," *J. Therm. Anal. Calorim.*, Dec. 2019, doi: 10.1007/s10973-019-09189-2.

[4] A. Battaglini, J. Lilliestam, A. Haas, and A. Patt, "Development of SuperSmart Grids for a more efficient utilisation of electricity from renewable sources," *J. Clean. Prod.*, vol. 17, no. 10, pp. 911–918, Jul. 2009, doi: 10.1016/j.jclepro.2009.02.006.

[5] F. Almonacid, C. Rus, P. J. Pérez, and L. Hontoria, "Estimation of the energy of a PV generator using

artificial neural network," *Renew. Energy*, vol. 34, no. 12, pp. 2743–2750, Dec. 2009, doi: 10.1016/j.renene.2009.05.020.

[6] W. B. Salem, B. Ayadi, and A. Mami, "Robust Diagnosis of a Fuel Cell Pumping System by Bond Graph Modeling Approach," *Int. J. Renew. Energy Res. IJRER*, vol. 11, no. 1, Art. no. 1, Mar. 2021.

[7] S. Chu and A. Majumdar, "Opportunities and challenges for a sustainable energy future," *Nature*, vol. 488, no. 7411, pp. 294–303, Aug. 2012, doi: 10.1038/nature11475.

[8] K. CHEN, S. Laghrouche, and A. Djerdir, "Proton Exchange Membrane Fuel Cell Degradation and Remaining Useful Life Prediction based on Artificial Neural Network," in *2018 7th International Conference on Renewable Energy Research and Applications (ICRERA)*, Oct. 2018, pp. 407–411. doi: 10.1109/ICRERA.2018.8567023.

[9] A. AlKassem, M. Al Ahmadi, and A. Draou, "Modeling and Simulation Analysis of a Hybrid PV-Wind Renewable Energy Sources for a Micro-Grid Application," in *2021 9th International Conference on Smart Grid (icSmartGrid)*, Jun. 2021, pp. 103–106. doi: 10.1109/icSmartGrid52357.2021.9551215.

[10] P. T. Bankupalli, S. Ghosh, L. Kumar, S. Samanta, and S. Jain, "Operational Adaptability of PEM Fuel Cell for Optimal Voltage Regulation With Maximum Power Extraction," *IEEE Trans. Energy Convers.*, vol. 35, no. 1, pp. 203–212, Mar. 2020, doi: 10.1109/TEC.2019.2949754.

[11] A. W. Al-Dabbagh, L. Lu, and A. Mazza, "Modelling, simulation and control of a proton exchange membrane fuel cell (PEMFC) power system," *Int. J. Hydrog. Energy*, vol. 35, no. 10, pp. 5061–5069, May 2010, doi: 10.1016/j.ijhydene.2009.08.090.

[12] S. L. Chavan and D. B. Talange, "Modeling and performance evaluation of PEM fuel cell by controlling its input parameters," *Energy*, vol. 138, pp. 437–445, Nov. 2017, doi: 10.1016/j.energy.2017.07.070.

[13] O. Aissa, S. Moulahoum, and I. Colak, "Intelligent Adaptive Control of the SAPF Intended to Improve the Power Grid Energy Quality," in *2021 9th International Conference on Smart Grid (icSmartGrid)*, Jun. 2021, pp. 76–81. doi: 10.1109/icSmartGrid52357.2021.9551237.

[14] S. Turkdogan, "Design and optimization of a solely renewable based hybrid energy system for residential electrical load and fuel cell electric vehicle," *Eng. Sci. Technol. Int. J.*, Sep. 2020, doi: 10.1016/j.jestch.2020.08.017.

[15] M. S. Alam and D. W. Gao, "Modeling and Analysis of a Wind/PV/Fuel Cell Hybrid Power System in HOMER," in *2007 2nd IEEE Conference on Industrial Electronics and Applications*, May 2007, pp. 1594–1599. doi: 10.1109/ICIEA.2007.4318677.

[16] N. Benyahia, H. Denoun, A. Badjiet, M. Zaouia, "MPPT controller for an interleaved boost dc–dc converter used in fuel cell electric vehicles," *Int. J. Hydrog. Energy*, vol. 39, no. 27, pp. 15196–15205, Sep. 2014, doi: 10.1016/j.ijhydene.2014.03.185.

[17] N. Benyahia, H. Denoun, M. Zaouia, T. Rekioua, and N. Benamrouche, "Power system simulation of fuel cell and supercapacitor based electric vehicle using an interleaving technique," *Int. J. Hydrog. Energy*, vol. 40, no. 45, pp. 15806–15814, Dec. 2015, doi: 10.1016/j.ijhydene.2015.03.081.

[18] S. Farhani, E. M. Barhoumi, and F. Bacha, "Design and hardware investigation of a new configuration of an isolated DC-DC converter for fuel cell vehicle," *Ain Shams Eng. J.*, Sep. 2020, doi: 10.1016/j.asej.2020.07.014.

[19] S. Farhani and F. Bacha, "Analysis. Design and Implementation of Fuel Cell LLC Resonant Converter Used in Electrical Vehicle," in *2018 15th International Multi-Conference on Systems, Signals Devices (SSD)*, Mar. 2018, pp. 310–315. doi: 10.1109/SSD.2018.8570517.

[20] E. Barhoumi, I. Ben Belgacem, A. Khiareddine, M. Zghaibeh, and I. Tlili, "A Neural Network-Based Four Phases Interleaved Boost Converter for Fuel Cell System Applications," *Energies*, vol. 11, no. 12, p. 3423, Dec. 2018, doi: 10.3390/en11123423.

[21] L. Gauchia, A. Bouscayrol, J. Sanz, R. Trigui, and P. Barrade, "Fuel cell, battery and supercapacitor hybrid system for electric vehicle: Modeling and control via energetic macroscopic representation," in *2011 IEEE Vehicle Power and Propulsion Conference*, Chicago, IL, USA, Sep. 2011, pp. 1–6. doi: 10.1109/VPPC.2011.6043246.

[22] F. Slah, A. Mansour, M. Hajer, and B. Faouzi, "Analysis, modeling and implementation of an interleaved boost DC-DC converter for fuel cell used in electric vehicle," *Int. J. Hydrog. Energy*, vol. 42, no. 48, pp. 28852–28864, Nov. 2017, doi: 10.1016/j.ijhydene.2017.08.068.

[23] S. Farhani and F. Bacha, "Modeling and control of a dc-dc resonant converter interfacing fuel cell in electric vehicle," in *2018 9th International Renewable Energy Congress (IREC)*, Mar. 2018, pp. 1–6. doi: 10.1109/IREC.2018.8362507.

[24] P. Abishri, "Review of Coupled Two and Three Phase Interleaved Boost Converter (IBC) and Investigation of Four Phase IBC for Renewable Application," p. 14, 2016.

[25] S. Gherairi "Zero-Emission Hybrid Electric System: Estimated Speed to Prioritize Energy Demand for Transport Applications," *Int. J. Smart Grid*, 2019, doi: 10.20508/ijsmartgrid.v3i4.76.g65.

[26] S. Farhani, A. N'Diaye, A. Djerdir, and F. Bacha, "Design and practical study of three phase interleaved boost converter for fuel cell electric vehicle," *J. Power*

Sources, vol. 479, p. 228815, Dec. 2020, doi: 10.1016/j.jpowsour.2020.228815.

[27] D. Guilbert, A. Gaillard, A. N'Diaye, and A. Djerdir, "Power switch failures tolerance and remedial strategies of a 4-leg floating interleaved DC/DC boost converter for photovoltaic/fuel cell applications," *Renew. Energy*, vol. 90, pp. 14–27, May 2016, doi: 10.1016/j.renene.2015.12.054.

[28] E. M. Barhoumi, S. Farhani, and F. Bacha, "High efficiency power electronic converter for fuel cell system application," *Ain Shams Eng. J.*, vol. 12, no. 3, pp. 2655–2664, Sep. 2021, doi: 10.1016/j.asej.2021.01.010.

[29] H. Wen and B. Su, "Hybrid-mode interleaved boost converter design for fuel cell electric vehicles," *Energy Convers. Manag.*, vol. 122, pp. 477–487, Aug. 2016, doi: 10.1016/j.enconman.2016.06.021.

[30] P. Thounthong, S. Raël, and B. Davat, "Control strategy of fuel cell/supercapacitors hybrid power sources for electric vehicle," *J. Power Sources*, vol. 158, no. 1, pp. 806–814, Jul. 2006, doi: 10.1016/j.jpowsour.2005.09.014.

[31] E. M. Barhoumi, M. Zghaibeh, P. C. Okonkwo, N. U. Hasan, S. Farhani, and F. Bacha, "Energy Management System for Photovoltaic-Battery-Fuel Cell using Arduino Board and Matlab Simulink," in *2022 IEEE Delhi Section Conference (DELCON)*, Feb. 2022, pp. 1–6. doi: 10.1109/DELCON54057.2022.9753625.

[32] D. Sankar, L. Syamala, B. Chembathu Ayyappan, and M. Kallarackal, "FPGA-Based Cost-Effective and Resource Optimized Solution of Predictive Direct Current Control for Power Converters," *Energies*, vol. 14, no. 22, Art. no. 22, Jan. 2021, doi: 10.3390/en14227669.

[33] P. T. Bankupalli, S. Ghosh, L. Kumar, and S. Samanta, "Fractional order modeling and two loop control of PEM fuel cell for voltage regulation considering both source and load perturbations," *Int. J. Hydrog. Energy*, vol. 43, no. 12, pp. 6294–6309, Mar. 2018, doi: 10.1016/j.ijhydene.2018.01.167.